Power-Oriented Modeling of Epicyclic Gear Trains

1st Roberto Zanasi
Department of Engineering "Enzo Ferrari"
University of Modena and Reggio Emilia
Modena, Italy
roberto.zanasi@unimore.it

2nd Davide Tebaldi
Department of Engineering "Enzo Ferrari"
University of Modena and Reggio Emilia
Modena, Italy
davide.tebaldi@unimore.it

***Abstract*—Model-based simulations are important in the automotive industry to study and evaluate the vehicle behavior. In this paper, the Power-Oriented Graphs (POG) technique is used as a tool for modeling epicyclic gear trains. A full elastic dynamic model of the system is first derived, which can then be reduced by neglecting the elastic contact points between the gears while still being able to recover the time behaviors of the spring tangential forces. The proposed modeling method is then applied to two epicyclic gear trains, and the design of a suitable control allowing to minimize the system dissipations is presented and applied to the second case study.**

***Index Terms*—Power-Oriented Graphs (POG), Epicyclic Gear Trains, Automotive, Control Design, Simulation**

I. Introduction

Epicyclic gear trains, also called planetary gear sets, are one of the most important devices employed in Power-Split Hybrid Electric Vehicles (HEVs). In the latter class of HEVs, see [1]-[2], epicyclic gear trains are typically used to enable the presence of contemporary power paths in the vehicle driveline. Depending on the Power-Split type, the epicyclic gear train can be located in different parts of the architecture [3], enabling different characteristics for the resulting vehicle topology.

One of the most challenging tasks with HEVs is the development of effective control strategies allowing to satisfy the power requirements of the vehicle while trying to minimize the engine fuel consumption; such issue is typically known in the literature as the "Energy Management Problem". Sufficiently accurate model-based simulations need to be performed to evaluate the effectiveness of a control strategy solution, which need to rely upon an accurate modeling of all the elements being present in the vehicle architecture. The modeling of epicyclic gear trains has been addressed in the literature using different approaches [4] - [6]. One of the most well-known and widespread modeling solutions is the lever analogy [7], from which the static and dynamic relations of epicyclic gear trains can be obtained. The modeling can also be performed using suitable graphical modeling techniques [8]. In this paper, the systematic approach for modeling planetary gears introduced in [9], which is based on the Power-Oriented Graphs (POG) modeling technique [10], is applied to two case studies: a Compound epicyclic gear train and a Coupled epicyclic gear train. The proposed approach allows to obtain the dynamic model of different epicyclic gear trains, which can be used for hybrid propulsion systems simulations together with the other physical elements models. Furthermore, the design of a suitable control to be applied to the epicyclic gear train is presented in this paper and tested in simulation, allowing to determine the optimal direction in the reduced model state space that gives the desired angular velocity while minimizing the dissipated power due to the internal dissipations.

This paper is structured as follows. Sec. II deals with the description of characteristics and basic properties of the POG modeling technique. In Sec. III, the notations of the presented modeling approach are given, the computation of the radius matrix uniquely defining the system is addressed, and the modeling of a Compound epicyclic gear train is performed. Sec. IV shows the modeling of the second case study, that is a Coupled epicyclic gear train, giving particular emphasis to the design of a suitable control allowing to minimize the internal dissipations. Finally, Sec. V gives the conclusions of this paper.

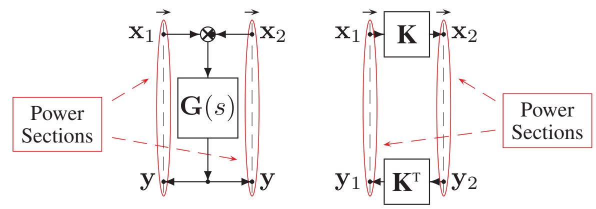

Fig. 1. POG elementary blocks: *elaboration block* and *connection block*.

TABLE I
Energetic domains: physical elements and power variables.

	Electrical	**Mech. Tras.**	**Mech. Rot.**	**Hydraulic**
D_e	Capacitor C	Mass M	Inertia J	Hyrd. Cap. C_I
v_e	Voltage V	Velocity $\dot{x}$	Ang. Velocity ω	Pressure P
D_f	Inductor L	Spring E	Rot. Spring E	Hydr. Ind. L_I
v_f	Current I	Force F	Torque τ	Vol. Flow Rate Q
R	Resistor R	Friction b	Ang. Friction b	Hydr. Res. R_I

II. The POG Modeling Technique

The Power-Oriented Graphs (POG) technique is a graphical modeling technique based on the same energetic approach employed by the Bond Graph (BG) technique, but refers to a different graphical notation. Power-Oriented Graphs are based on the usage of two elementary blocks, namely the elaboration block and the connection block, as shown in Fig. 1. The first one is used to model all the physical elements storing and/or dissipating energy, whereas the second one is used to model all the physical elements performing lossless energy conversion.

The elaboration block can be static or dynamic, and is described by the transfer function $G(s)$ (or the transfer matrix $\mathbf{G}(s)$) of the considered physical element. A static element is characterized by a constant transfer function $G(s) = R$ and describes a static relation between the input variable v_f and the output variable v_e or viceversa. The dynamic elements can be classified into *across elements* D_e, having a flow variable v_f as input and an across variable v_e as output, and *flow elements* D_f, having an across variable v_e as input and a flow variable v_f as output. An across power variable v_e is always defined between two points, whereas a flow power variable v_f is defined in each point of the space. Table I provides a compact description of the dynamic and static elements, as well as the across and flow variables, in the four typically considered energetic domains. The crossed circle in the upper part of the elaboration block in Fig. 1 is a *summation node*, where the black spot present on the right means that the power variable entering from that side of the summation node has to be subtracted.

The connection block is characterized by a coefficient K (or a matrix $\mathbf{K}$) which completely describes the energy conversion between two different energetic domains.

One of the main characteristics of the POG modeling technique is to maintain a direct correspondence between the power sections in the model, highlighted by the red ellipses in Fig. 1, and the power sections of the actual system. The scalar product $\mathbf{x}^{\mathrm{T}}\mathbf{y}$ of the two power variables $\mathbf{x}$ and $\mathbf{y}$ has the physical meaning of *power flowing through the considered section*. The black oriented arrows located at the top of each power section in Fig. 1 indicate the positive direction of the power flows through the corresponding power section.

Any physical system modeled using the POG technique can be written in a POG state-space representation as follows:

$$\begin{cases} \mathbf{L}\,\dot{\mathbf{x}} = \mathbf{A}\,\mathbf{x} + \mathbf{B}\,\mathbf{u} \\ \mathbf{y} = \mathbf{C}\,\mathbf{x} + \mathbf{D}\,\mathbf{u} \end{cases},$$

where $\mathbf{L}$ is the energy matrix, $\mathbf{A}$ is the power matrix, $\mathbf{B}$ is the input matrix, $\mathbf{C}$ is the output matrix and $\mathbf{D}$ is the input-output matrix. The energy matrix $\mathbf{L}$ and the power matrix $\mathbf{A}$ describe the energy E_s stored in the system and the power P_d dissipated in the system, respectively:

$$E_s = \frac{1}{2}\,\mathbf{x}^{\mathrm{T}}\,\mathbf{L}\,\mathbf{x}, \qquad\qquad P_d = \mathbf{x}^{\mathrm{T}}\,\mathbf{A}_s\,\mathbf{x},$$

where $\mathbf{A}_s$ is the symmetric part of matrix $\mathbf{A}$.

When an eigenvalue of the energy matrix $\mathbf{L}$ tends to zero or to infinite, the system model degenerates to a lower dimension, and the reduced model can be obtained by applying a proper congruent transformation $\mathbf{x} = \mathbf{T}_1\,\mathbf{x}_1$, where $\mathbf{x}$ is the original full model state vector and $\mathbf{x}_1$ is the state vector of the new reduced model. The new matrices of the reduced model can be directly obtained as follows: $\mathbf{L}_1 = \mathbf{T}_1^{\mathrm{T}}\,\mathbf{L}\,\mathbf{T}_1$, $\mathbf{A}_1 = \mathbf{T}_1^{\mathrm{T}}\,\mathbf{A}\,\mathbf{T}_1$, $\mathbf{B}_1 = \mathbf{T}_1^{\mathrm{T}}\,\mathbf{B}$, $\mathbf{C}_1 = \mathbf{C}\,\mathbf{T}_1$ and $\mathbf{D}_1 = \mathbf{D}$.

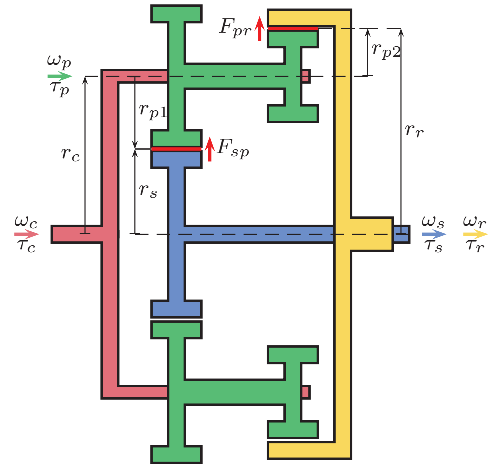

Fig. 2. Structure of the considered Compound epicyclic gear train.

III. Modeling a compound epicyclic gear train

The modeling of the Compound epicyclic gear train of Fig. 2 is performed in this section. Within the figure, a specific color and a one-digit subscript "i" have been assigned to each inertial element, that is to each rotating gear. Subscript "i" also denotes all the parameters associated with the i-th gear: its moment of inertia J_i, its linear friction coefficient b_i, its angular velocity ω_i and its input torque τ_i. Similarly, a two-digit subscript "ij" has been assigned to each tangential spring representing the gears elastic contact points, which are denoted in Fig. 2 by red lines (i.e. "▬"). Subscript "ij" also denotes all the parameters associated with the ij-th tangential spring: its stiffness K_{ij}, its linear friction coefficient b_{ij} and the tangential force F_{ij} it generates.

Two types of color oriented arrows are present within Fig. 2:

- horizontal arrows (e.g. "→") highlighting the rotation axes and the positive directions of angular velocities ω_i and of input torques τ_i, for $i \in \{c, p, s, r\}$.
- vertical arrows (e.g. " ↓) highlighting the positive directions of the tangential forces F_{ij}, for $ij \in \{sp, pr\}$.

The dynamic equations of the considered system are described by the following POG state-space form, see [9]- [10]:

$$\begin{cases} \mathbf{L}\,\dot{\mathbf{x}} = \mathbf{A}\,\mathbf{x} + \mathbf{B}\,\mathbf{u} \\ \mathbf{y} = \mathbf{B}^{\mathrm{T}}\,\mathbf{x} \end{cases}, \qquad \mathbf{x} = \begin{bmatrix} \boldsymbol{\omega} \\ \mathbf{F} \end{bmatrix}, \qquad \mathbf{B} = \begin{bmatrix} \mathbf{I} \\ \mathbf{0} \end{bmatrix}. \tag{1}$$

whose graphical representation is given by the POG scheme in Fig. 3. Within system (1), $\mathbf{x}$, $\mathbf{u} = \boldsymbol{\tau}$, $\mathbf{y} = \boldsymbol{\omega}$ are the state, input and output vectors of the system, respectively, $\mathbf{B}$ is the input matrix and $\mathbf{I}$ is an identity matrix of proper dimension. The energy and power matrices $\mathbf{L}$ and $\mathbf{A}$ have the following structure:

$$\mathbf{L} = \begin{bmatrix} \mathbf{J} & \mathbf{0} \\ \mathbf{0} & \mathbf{K}^{\text{-1}} \end{bmatrix}, \qquad \mathbf{A} = \begin{bmatrix} -\mathbf{B}_J - \mathbf{R}^{\mathrm{T}}\mathbf{B}_k\mathbf{R} & -\mathbf{R}^{\mathrm{T}} \\ \mathbf{R} & \mathbf{0} \end{bmatrix}. \tag{2}$$

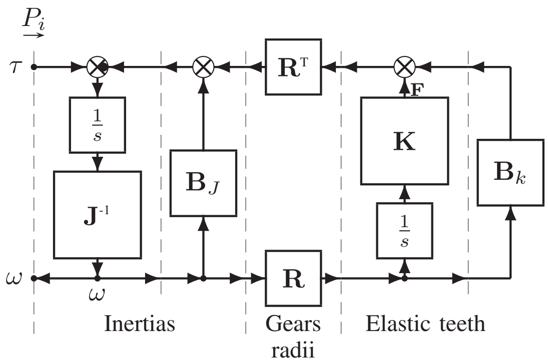

Fig. 3. POG scheme of epicyclic gear trains.

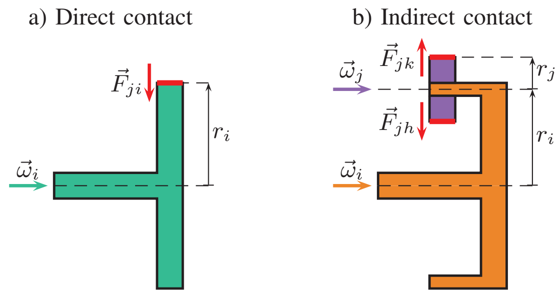

Fig. 4. *Effective radius* r_i: a) Direct contact; b) Indirect contact.

The velocity vector $\boldsymbol{\omega}$, the input vector $\mathbf{u} = \boldsymbol{\tau}$, the inertial matrix $\mathbf{J}$ and the inertial friction matrix $\mathbf{B}_J$ are defined as:

$$\boldsymbol{\omega}=\begin{bmatrix}\omega_c\\ \omega_p\\ \omega_s\\ \omega_r\end{bmatrix}, \boldsymbol{\tau}=\begin{bmatrix}\tau_c\\ \tau_p\\ \tau_s\\ \tau_r\end{bmatrix}, \mathbf{J}=\begin{bmatrix}J_c & 0 & 0 & 0\\ 0 & J_p & 0 & 0\\ 0 & 0 & J_s & 0\\ 0 & 0 & 0 & J_r\end{bmatrix}, \mathbf{B}_J=\begin{bmatrix}b_c & 0 & 0 & 0\\ 0 & b_p & 0 & 0\\ 0 & 0 & b_s & 0\\ 0 & 0 & 0 & b_r\end{bmatrix}. \quad (3)$$

The force vector $\mathbf{F}$, the stiffness matrix $\mathbf{K}$ and stiffness friction matrix $\mathbf{B}_K$ are defined as:

$$\mathbf{F}=\begin{bmatrix}F_{sp} & F_{pr}\end{bmatrix}^T, \quad \mathbf{K}=\begin{bmatrix}K_{sp} & 0\\ 0 & K_{pr}\end{bmatrix}, \quad \mathbf{B}_K=\begin{bmatrix}b_{sp} & 0\\ 0 & b_{pr}\end{bmatrix}. \quad (4)$$

From (3), it can be noticed that the position of angular velocities ω_i within vector $\boldsymbol{\omega}$ completely defines the position of input torques τ_i within vector $\boldsymbol{\tau}$ and of parameters J_i and b_i within matrices $\mathbf{J}$ and $\mathbf{B}_J$, respectively. From (4), it can be noticed that the position of tangential forces F_{ij} within vector $\mathbf{F}$ completely defines the position of parameters K_{ij} and b_{ij} within matrices $\mathbf{K}$ and $\mathbf{B}_K$, respectively. The only matrix uniquely defining system (1) is the radius matrix $\mathbf{R}$. With reference to the Compound epicyclic gear train of Fig. 2, and applying the procedure described in Sec. III-A, matrix $\mathbf{R}$ assumes the following form:

$$\begin{array}{cc} & \begin{array}{cccc} c & p & s & r \end{array} \\ \begin{array}{c} sp \\ pr \end{array} \mathbf{R} = & \begin{bmatrix} -r_c & r_{p1} & r_s & 0 \\ r_c & r_{p2} & 0 & -r_r \end{bmatrix} \end{array} \quad (5)$$

The green coefficients along the rows and the columns of matrix $\mathbf{R}$ in (5) denote the subscripts of the state space variables ω_i and F_{ij}, respectively.

A. Computation of the radius matrix R.

Let $r_{ij,i}$ denote the generic coefficient of matrix $\mathbf{R} = [r_{ij,i}]$ in (5), linking the tangential force $\vec{F}_{ij}$ to the angular velocity $\vec{\omega}_i$. Coefficient $r_{ij,i}$ can be expressed as:

$$r_{ij,i} = S_{F_{ij}}\, S_{\omega_i}\, r_i$$

where r_i, $S_{F_{ij}}$ and S_{ω_i} are:

1) r_i is the *effective radius* of angular velocity $\vec{\omega}_i$. Two different cases can occur: a) velocity $\vec{\omega}_i$ directly affecting the force vector $\vec{F}_{ij}$, see Fig. 4.a, in which case the *effective radius* r_i coincides with the radius of the gear associated with velocity $\vec{\omega}_i$; b) velocity $\vec{\omega}_i$ affecting the force vector $\vec{F}_{ij}$ through an intermediate gear "j", see Fig. 4.b, in which case the *effective radius* r_i coincides with the distance between the rotation axes of the two angular velocities $\vec{\omega}_i$ and $\vec{\omega}_j$.
2) $S_{F_{ij}}$ is the sign of the positive orientation of vector $\vec{F}_{ij}$:

$$S_{F_{ij}} = \begin{cases} 1 & \text{if } \vec{F}_{ij} \text{ is oriented from gear } i \text{ to gear } j \\ -1 & \text{if } \vec{F}_{ji} \text{ is oriented from gear } j \text{ to gear } i \end{cases}$$

3) S_{ω_i} is related to the sign of the velocity vector $\vec{\omega}_i$:

$$S_{\omega_i} = \begin{cases} 1 & \text{if } \vec{F}_{ij} \text{ is on the left of vector } \vec{\omega}_i \\ -1 & \text{if } \vec{F}_{ij} \text{ is on the right of vector } \vec{\omega}_i \end{cases}$$

The left and right sides of vector $\vec{\omega}_i$ are determined by moving in the positive direction along vector $\vec{\omega}_i$.

B. Calculation of the reduced rigid model.

When all $K_{ij} \to \infty$ in matrix $\mathbf{K}$, from model (1) it results:

$$\mathbf{R}\,\omega = 0 \quad \Leftrightarrow \quad \begin{cases} r_{p1}\,\omega_p - r_c\,\omega_c + r_s\,\omega_s = 0 \\ r_c\,\omega_c + r_{p2}\,\omega_p - r_r\,\omega_r = 0 \end{cases}, \quad (6)$$

meaning that vector $\boldsymbol{\omega}$ can be expressed as a function of two angular velocities. Choosing $\mathbf{x}_1 = \begin{bmatrix}\omega_s & \omega_c\end{bmatrix}^{\mathrm{T}}$, it results:

$$\underbrace{\begin{bmatrix}\boldsymbol{\omega}\\ \mathbf{F}\end{bmatrix}}_{\mathbf{x}} = \underbrace{\begin{bmatrix}\mathbf{Q}_1\\ \mathbf{0}\end{bmatrix}}_{\mathbf{T}_1} \underbrace{\begin{bmatrix}\omega_s\\ \omega_c\end{bmatrix}}_{\mathbf{x}_1}, \qquad \underbrace{\begin{bmatrix}\omega_c\\ \omega_p\\ \omega_s\\ \omega_r\end{bmatrix}}_{\boldsymbol{\omega}} = \underbrace{\begin{bmatrix}0 & 1\\ -\frac{r_s}{r_{p1}} & \frac{r_c}{r_{p1}}\\ 1 & 0\\ -\frac{r_{p2} r_s}{r_{p1} r_r} & \frac{r_c r_{p1} + r_c r_{p2}}{r_{p1} r_r}\end{bmatrix}}_{\mathbf{Q}_1} \underbrace{\begin{bmatrix}\omega_s\\ \omega_c\end{bmatrix}}_{\mathbf{x}_1}$$

By applying the congruent transformation $\mathbf{x} = \mathbf{T}_1\mathbf{x}_1$ to system (1), see [10], one obtains the following reduced rigid state-space model:

$$\mathbf{L}_1\dot{\mathbf{x}}_1 = \mathbf{A}_1\mathbf{x}_1 + \mathbf{B}_1\mathbf{u}, \quad (7)$$

where matrices $\mathbf{L}_1$, $\mathbf{A}_1$ and $\mathbf{B}_1$ have the following structure:

$$\begin{cases} \mathbf{L}_1 = \mathbf{T}_1^{\mathrm{T}}\mathbf{L}\,\mathbf{T}_1 = \mathbf{Q}_1^{\mathrm{T}}\mathbf{J}\,\mathbf{Q}_1 \\ \mathbf{A}_1 = \mathbf{T}_1^{\mathrm{T}}\mathbf{A}\,\mathbf{T}_1 = -\mathbf{Q}_1^{\mathrm{T}}\mathbf{B}_J\mathbf{Q}_1 \\ \mathbf{B}_1 = \mathbf{T}_1^{\mathrm{T}}\mathbf{B} = \mathbf{Q}_1^{\mathrm{T}} \end{cases} \quad (8)$$

For the considered Compound epicyclic gear train system it is: $\mathbf{L}_1 \in \mathcal{R}^{2\times 2}$, $\mathbf{A}_1 \in \mathcal{R}^{2\times 2}$ and $\mathbf{B}_1 = \mathbf{Q}_1^{\mathrm{T}} \in \mathcal{R}^{2\times 4}$.

TABLE II
COMPOUND EPICYCLIC GEAR TRAIN: SIMULATION PARAMETERS.

$r_{p1} = 9$ cm	$r_{p2} = 6$ cm
$r_s = 12$ cm	$r_c = 21$ cm
$r_r = 27$ cm	$J_c = 357423.3$ kg mm^2
$J_p = 156754.2$ kg mm^2	$J_s = 91462.3$ kg mm^2
$J_r = 2344077.9$ kg mm^2	$b_c = 0.4$ Nm/rpm
$b_p = 0.4$ Nm/rpm	$b_s = 0.4$ Nm/rpm
$b_r = 0.4$ Nm/rpm	$K_{sp} = 5 \cdot 10^5$ N/mm
$K_{pr} = 5 \cdot 10^5$ N/mm	$d_{sp} = 0.8$ N s/cm
$d_{pr} = 0.8$ N s/cm	$\boldsymbol{\omega}_0 = [\ 0\ \ 0\ \ 0\ \ 0\ ]$ rpm
$\mathbf{F}_0 = [\ 0\ \ 0\ ]$ N	$\boldsymbol{\tau} = [\ 100\ \ 0\ \ 0\ \ 0\ ]$ Nm

C. Calculation of the vector force $\mathbf{F}$.

It can be proven, see [9], that vector $\mathbf{F}$ can be obtained from the reduced rigid system (7) as follows:

$$\mathbf{F} = (\mathbf{R}\mathbf{R}^{\mathrm{T}})^{-1}\mathbf{R}(\boldsymbol{\tau} - \mathbf{J}\mathbf{Q}_1\dot{\mathbf{x}}_1 - \mathbf{B}_J\mathbf{Q}_1\mathbf{x}_1). \tag{9}$$

Eq. (9) gives the tangential forces F_{ij} at the gears contact points as a function of the input vector $\boldsymbol{\tau}$, the state vector $\mathbf{x}_1$ of the reduced rigid model (7) and its first derivative $\dot{\mathbf{x}}_1$.

D. Compound epicyclic gear train: simulation results.

The full model (1) and the reduced model (7) of the Compound epicyclic gear train have been simulated using the parameters and initial conditions given in Tab. II. Note that any power section (ω_i, τ_i), for $i \in \{c, p, s, r\}$, can potentially be either an input or an output, depending on the powertrain configuration on which the considered epicyclic gear train is mounted. In the considered case, since the objective of the simulation is simply to show the effectiveness of the reduced model compared to the full one, an input motive torque is applied to the power section characterized by subscript "c", see vector $\boldsymbol{\tau}$ in Tab. II, whereas the inertial elements corresponding to the remaining power sections are disconnected. The obtained simulation results are shown in Fig. 5. The left subplot of Fig. 5 shows the angular velocities ω_i, for $i \in \{c, p, s, r\}$, whereas the right subplot of Fig. 5 shows the time behavior of the tangential forces F_{ij}, for $ij \in \{sp, pr\}$. For both subplots, the colored characteristics refer to the simulation performed on the full elastic model (1), whereas the red dashed characteristics refer to the simulation performed on the reduced model (7). As for the latter, the red dashed characteristics of tangential forces F_{ij} have been computed using Eq. (9). From Fig. 5, it is possible to appreciate the good matching of the results given by the full and reduced models. Furthermore, a comparison in terms of simulation time has been made, by performing ten simulations of the full and reduced models of the Compound epicyclic gear train with the same ode45 variable-step size solver, using the parameters and initial conditions given in Tab. II. The resulting average simulation time for the full and reduced models are 0.161 s and 0.140 s, respectively, leading to a reduction in terms of simulation time of the reduced model with respect to the full model of 12.5 %. This reduction is mainly due to two factors: 1) Eq. (9) can be implemented offline; 2)

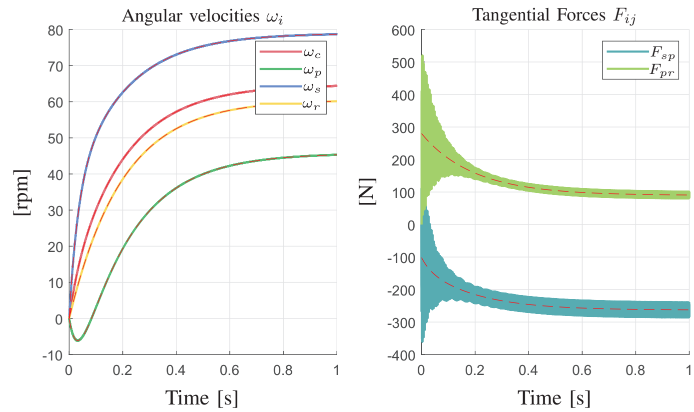

Fig. 5. Simulation of the Compound epicyclic gear train: angular velocities ω_i (left subplot) and tangential forces F_{ij} (right subplot).

The reduced rigid model (7) does not contain any tangential spring. Note that as the number of gears contact points, and thus of tangential springs, present within the system increases, i.e. when considering more complex epicyclic gear trains, the simulation time of the full model is expected to increase. Similarly, if the springs stiffness coefficients increase, that is if the full model becomes more rigid, the simulation time of the full model is expected to increase as well, as shorter step sizes are required to accurately simulate fast dynamics.

IV. MODELING A COUPLED EPICYCLIC GEAR TRAIN

The modeling of the Coupled epicyclic gear train of Fig. 6 is performed in this section. The full and reduced models of the system can still be described by (1) and (7), and the new system matrices and vectors are defined in the following.

The velocity vector $\boldsymbol{\omega}$, the input vector $\mathbf{u} = \boldsymbol{\tau}$, the inertial matrix $\mathbf{J}$ and the inertial friction matrix $\mathbf{B}_J$ are defined as:

$$\boldsymbol{\omega} = \begin{bmatrix} \omega_a \\ \omega_c \\ \omega_p \\ \omega_s \\ \omega_b \\ \omega_r \end{bmatrix}, \boldsymbol{\tau} = \begin{bmatrix} \tau_a \\ \tau_c \\ \tau_p \\ \tau_s \\ \tau_b \\ \tau_r \end{bmatrix}, \mathbf{J} = \begin{bmatrix} J_a & 0 & 0 & 0 & 0 & 0 \\ 0 & J_c & 0 & 0 & 0 & 0 \\ 0 & 0 & J_p & 0 & 0 & 0 \\ 0 & 0 & 0 & J_s & 0 & 0 \\ 0 & 0 & 0 & 0 & J_b & 0 \\ 0 & 0 & 0 & 0 & 0 & J_r \end{bmatrix}, \mathbf{B}_J = \begin{bmatrix} b_a & 0 & 0 & 0 & 0 & 0 \\ 0 & b_c & 0 & 0 & 0 & 0 \\ 0 & 0 & b_p & 0 & 0 & 0 \\ 0 & 0 & 0 & b_s & 0 & 0 \\ 0 & 0 & 0 & 0 & b_b & 0 \\ 0 & 0 & 0 & 0 & 0 & b_r \end{bmatrix}$$

The force vector $\mathbf{F}$, the stiffness matrix $\mathbf{K}$ and stiffness friction matrix $\mathbf{B}_K$ are defined as:

$$\mathbf{F} = \begin{bmatrix} F_{ps} \\ F_{pr} \\ F_{br} \\ F_{ba} \end{bmatrix}, \mathbf{K} = \begin{bmatrix} K_{ps} & 0 & 0 & 0 \\ 0 & K_{pr} & 0 & 0 \\ 0 & 0 & K_{br} & 0 \\ 0 & 0 & 0 & K_{ba} \end{bmatrix}, \mathbf{B}_K = \begin{bmatrix} b_{ps} & 0 & 0 & 0 \\ 0 & b_{pr} & 0 & 0 \\ 0 & 0 & b_{br} & 0 \\ 0 & 0 & 0 & b_{ba} \end{bmatrix}$$

Applying the rules given in Sec. III-A, matrix $\mathbf{R}$ results:

$$\begin{array}{c} \\ ps \\ pr \\ br \\ ba \end{array} \mathbf{R} = \begin{array}{c} \begin{array}{cccccc} a & c & p & s & b & r \end{array} \\ \begin{bmatrix} 0 & r_c & -r_p & -r_{s1} & 0 & 0 \\ 0 & r_c & r_p & 0 & 0 & -r_{r1} \\ 0 & 0 & 0 & r_{s2} & r_b & -r_{r2} \\ -r_a & 0 & 0 & r_{s2} & -r_b & 0 \end{bmatrix} \end{array} \tag{10}$$

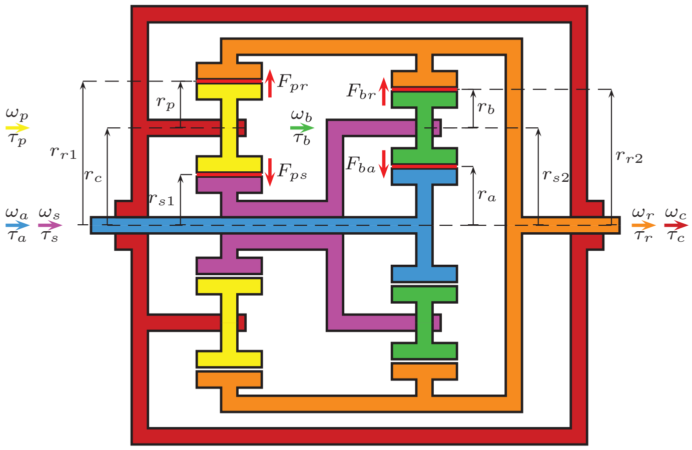

Fig. 6. Structure of the considered Coupled epicyclic gear train.

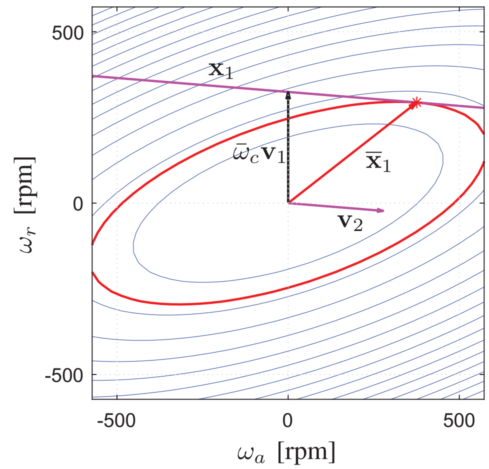

Fig. 7. Optimal condition $\overline{\mathbf{x}}_1$ minimizing the dissipated power P_d.

When all $K_{ij} \to \infty$ in matrix $\mathbf{K}$, from model (1) it results:

$$\mathbf{R}\,\boldsymbol{\omega} = \mathbf{0} \quad \Leftrightarrow \quad \begin{cases} r_c\,\omega_c - r_p\,\omega_p - r_{s1}\,\omega_s = 0 \\ r_c\,\omega_c + r_p\,\omega_p - r_{r1}\,\omega_r = 0 \\ r_b\,\omega_b - r_{r2}\,\omega_r + r_{s2}\,\omega_s = 0 \\ r_{s2}\,\omega_s - r_b\,\omega_b - r_a\,\omega_a = 0 \end{cases} \tag{11}$$

Choosing $\mathbf{x}_1 = \begin{bmatrix} \omega_a & \omega_r \end{bmatrix}^{\mathrm{T}}$ as reduced state vector, one obtains:

$$\underbrace{\begin{bmatrix} \boldsymbol{\omega} \\ \mathbf{F} \end{bmatrix}}_{\mathbf{x}} = \underbrace{\begin{bmatrix} \mathbf{Q}_1 \\ \mathbf{0} \end{bmatrix}}_{\mathbf{T}_1} \underbrace{\begin{bmatrix} \omega_a \\ \omega_r \end{bmatrix}}_{\mathbf{x}_1}, \quad \underbrace{\begin{bmatrix} \omega_a \\ \omega_c \\ \omega_p \\ \omega_s \\ \omega_b \\ \omega_r \end{bmatrix}}_{\boldsymbol{\omega}} = \underbrace{\begin{bmatrix} 1 & 0 \\ \frac{r_a r_{s1}}{4 r_c r_{s2}} & \frac{2 r_{r1} r_{s2} + r_{r2} r_{s1}}{4 r_c r_{s2}} \\ -\frac{r_a r_{s1}}{4 r_p r_{s2}} & \frac{2 r_{r1} r_{s2} - r_{r2} r_{s1}}{4 r_p r_{s2}} \\ \frac{r_a}{2 r_{s2}} & \frac{r_{r2}}{2 r_{s2}} \\ -\frac{r_a}{2 r_b} & \frac{r_{r2}}{2 r_b} \\ 0 & 1 \end{bmatrix}}_{\mathbf{Q}_1} \underbrace{\begin{bmatrix} \omega_a \\ \omega_r \end{bmatrix}}_{\mathbf{x}_1} \tag{12}$$

where the structure of the reduced rigid model is the same as the one given in (7) and (8).

A. Coupled epicyclic gear train: control design

Let us refer to the reduced rigid model (7) obtained using (12). Let us use the two velocities ω_a and ω_r in order to obtain a desired value $\bar{\omega}_c$ for the angular velocity ω_c. From (12), it follows that:

$$\bar{\omega}_c = q_1\,\omega_a + q_2\,\omega_r = \underbrace{\begin{bmatrix} q_1 & q_2 \end{bmatrix}}_{\mathbf{q}_1^{\mathrm{T}}} \underbrace{\begin{bmatrix} \omega_a \\ \omega_r \end{bmatrix}}_{\mathbf{x}_1} = \mathbf{q}_1^{\mathrm{T}}\,\mathbf{x}_1 \tag{13}$$

where:

$$q_1 = \frac{r_a r_{s1}}{4 r_c r_{s2}}, \qquad q_2 = \frac{2 r_{r1} r_{s2} + r_{r2} r_{s1}}{4 r_c r_{s2}}. \tag{14}$$

All the solutions $\mathbf{x}_1$ of the linear system (13) can be expressed as follows:

$$\mathbf{x}_1 = \bar{\omega}_c\,\mathbf{v}_1 + \alpha\,\mathbf{v}_2, \tag{15}$$

where $\mathbf{v}_1$ is any particular solution of equation $1 = \mathbf{q}_1^{\mathrm{T}}\,\mathbf{v}_1$, $\mathbf{v}_2$ is any particular vector such that $\mathbf{v}_2 \in \ker(\mathbf{q}_1^{\mathrm{T}})$, and $\alpha \in \mathcal{R}$. Possible values for vectors $\mathbf{v}_1$ and $\mathbf{v}_2$ are:

$$\mathbf{v}_1 = \begin{bmatrix} \frac{1}{q_1} \\ 0 \end{bmatrix}, \qquad \mathbf{v}_1 = \begin{bmatrix} 0 \\ \frac{1}{q_2} \end{bmatrix}, \qquad \mathbf{v}_2 = \begin{bmatrix} q_2 \\ -q_1 \end{bmatrix}.$$

The dissipated power P_d of the POG reduced rigid model (7) along the solutions (15) can be expressed as follows:

$$P_d = \mathbf{x}_1^{\mathrm{T}} \mathbf{A}_1 \mathbf{x}_1 = (\bar{\omega}_c \mathbf{v}_1 + \alpha\,\mathbf{v}_2)^{\mathrm{T}} \mathbf{A}_1 (\bar{\omega}_c \mathbf{v}_1 + \alpha\,\mathbf{v}_2) \tag{16}$$

Since matrix $\mathbf{A}_1$ in (7) is symmetric, the partial derivative of the dissipated power P_d with respect to α is:

$$\frac{\partial P_d}{\partial \alpha} = 2\,\mathbf{v}_2^{\mathrm{T}} \mathbf{A}_1 (\bar{\omega}_c \mathbf{v}_1 + \alpha\,\mathbf{v}_2) \tag{17}$$

The optimal solution in (15) minimizing the dissipated power P_d can be obtained from (17) as follows:

$$\frac{\partial P_d}{\partial \alpha} = 0 \qquad \Rightarrow \qquad \alpha^* = -\bar{\omega}_c \frac{\mathbf{v}_2^{\mathrm{T}} \mathbf{A}_1 \mathbf{v}_1}{\mathbf{v}_2^{\mathrm{T}} \mathbf{A}_1 \mathbf{v}_2}. \tag{18}$$

Substituting α^* in (15) one obtains:

$$\overline{\mathbf{x}}_1 = \begin{bmatrix} \bar{\omega}_a \\ \bar{\omega}_r \end{bmatrix} = \bar{\omega}_c \underbrace{\left(\mathbf{v}_1 - \frac{\mathbf{v}_2^{\mathrm{T}} \mathbf{A}_1 \mathbf{v}_1}{\mathbf{v}_2^{\mathrm{T}} \mathbf{A}_1 \mathbf{v}_2} \mathbf{v}_2 \right)}_{\vec{\mathbf{x}}_{1c}} = \bar{\omega}_c\,\vec{\mathbf{x}}_{1c}. \tag{19}$$

One can easily prove that vector $\vec{\mathbf{x}}_{1c}$ does not depend on the particular choice of parameter $\bar{\omega}_c$ and of vectors $\mathbf{v}_1$ and $\mathbf{v}_2$. Vector $\mathbf{x}_1 = \overline{\mathbf{x}}_1$ is the solution of equation (13) for which the power P_d dissipated in the system is minimum. This optimal condition is shown in Fig. 7: the blue lines are the contour ellipses associated with the dissipated power P_d in (16) when the parameters reported in Tab. III are used, the magenta straight line $\mathbf{x}_1$ is the set (15) of all the solutions of equation (13), vector $\overline{\mathbf{x}}_1$ is the optimal solution minimizing the dissipated power P_d, the red ellipse is the contour line where the dissipated power P_d is minimum with respect to the all possible solutions $\mathbf{x}_1$.

TABLE III

COUPLED EPICYCLIC GEAR TRAIN: SIMULATION PARAMETERS.

$r_a = 10.5$ cm	$r_b = 7.5$ cm
$r_p = 9$ cm	$r_{s1} = 9.6$ cm
$r_c = 18.6$ cm	$r_{r1} = 27.6$ cm
$r_{s2} = 18$ cm	$r_{r2} = 25.5$ cm
$J_a = 58081.3$ kg mm^2	$J_c = 2199669.9$ kg mm^2
$J_p = 26527.6$ kg mm^2	$J_s = 501613.4$ kg mm^2
$J_b = 11630$ kg mm^2	$J_r = 3199361.6$ kg mm^2
$b_a = 0.3$ Nm/rpm	$b_c = 0.18$ Nm/rpm
$b_p = 0.28$ Nm/rpm	$b_s = 0.14$ Nm/rpm
$b_b = 0.51$ Nm/rpm	$b_r = 0.12$ Nm/rpm
$K_{ba} = 20$ N/mm	$K_{ps} = 20$ N/mm
$K_{pr} = 20$ N/mm	$K_{br} = 20$ N/mm
$d_{ba} = 1.8$ N s/cm	$d_{ps} = 1.8$ N s/cm
$d_{pr} = 1.8$ N s/cm	$d_{br} = 1.8$ N s/cm

The reduced system $\mathbf{L}_1\dot{\mathbf{x}}_1 = \mathbf{A}_1\mathbf{x}_1 + \mathbf{B}_1\mathbf{u}$ in (7) controlled using the input vector $\mathbf{u} = \begin{bmatrix} \tau_a & 0 & 0 & 0 & 0 & \tau_r \end{bmatrix}^{\mathsf{T}}$ simplifies as follows:

$$\mathbf{L}_1\dot{\mathbf{x}}_1 = \mathbf{A}_1\mathbf{x}_1 + \boldsymbol{\tau}_1, \qquad \boldsymbol{\tau}_1 = \begin{bmatrix} \tau_a \\ \tau_r \end{bmatrix}. \tag{20}$$

One can easily verify that using the following control law:

$$\boldsymbol{\tau}_1 = -\mathbf{A}_1\mathbf{x}_1 + \mathbf{L}_1[\dot{\overline{\mathbf{x}}}_1 - \mathbf{K}\,(\overline{\mathbf{x}}_1 - \mathbf{x}_1)] \tag{21}$$

system (20) simplifies as follows:

$$\dot{\overline{\mathbf{x}}}_1 - \dot{\mathbf{x}}_1 = \mathbf{K}\,(\overline{\mathbf{x}}_1 - \mathbf{x}_1) \tag{22}$$

where $\mathbf{K} = \mathrm{diag}([k_1 \;\; k_2])$ is a proper constant matrix to be designed. From (22), it is easy to see that the two parameters k_l and k_2 of matrix $\mathbf{K}$ are equal to the two eigenvalues λ_1 and λ_2 of system (22): $k_1 = \lambda_1$, $k_2 = \lambda_2$.

B. Coupled epicyclic gear train: simulation results

The Coupled epicyclic gear train shown in Fig. 6 has been simulated using the reduced rigid system (7), the parameters shown in Tab. III, the initial conditions $\boldsymbol{\omega}_0 = [\,0\;0\;0\;0\;0\;0\,]$rpm, $\mathbf{F}_0 = [\,0\;0\;0\;0\,]$N, the control law given in (21), the design parameters $k_1 = \lambda_1 = -10$, $k_2 = \lambda_2 = -10$ and the desired angular velocity $\bar{\omega}_c = 300$ rpm. According to the definition of vector $\boldsymbol{\tau}$ in (20), which is employed in the control law in (21), one can notice that the two torques applied to the power sections characterized by subscripts "a" and "r" are those employed as control inputs for the considered case study, whereas the inertial elements corresponding to the remaining power sections are disconnected. The numeric values of matrices $\mathbf{L}_1$ are $\mathbf{A}_1$ are the following:

$$\mathbf{L}_1 = \begin{bmatrix} 0.119 & 0.238 \\ 0.238 & 5.401 \end{bmatrix}, \quad \mathbf{A}_1 = \begin{bmatrix} -5.42 & 5.85 \\ 5.85 & -20.84 \end{bmatrix}.$$

Vector $\mathbf{q}_1$ in (13) is characterized by the following parameters: $q_1 = 0.0753$ and $q_2 = 0.9247$. The obtained simulations results are shown in Fig. 8: the angular velocities ω_i are reported on the left subplot and the tangential forces F_{ij} are reported on the right subplot. The tangential forces F_{ij} have been computed using Eq. (9). From Fig. 8, one can appreciate the good control of the desired angular velocity $\bar{\omega}_c = 300$ rpm obtained using the control law (21). Note that the transient is aperiodic and the settling time $T_s \simeq \frac{3}{\lambda} \simeq 0.34$ is congruent with the choice of the two coincident real eigenvalues in $\lambda_1 = \lambda_2 = -10$.

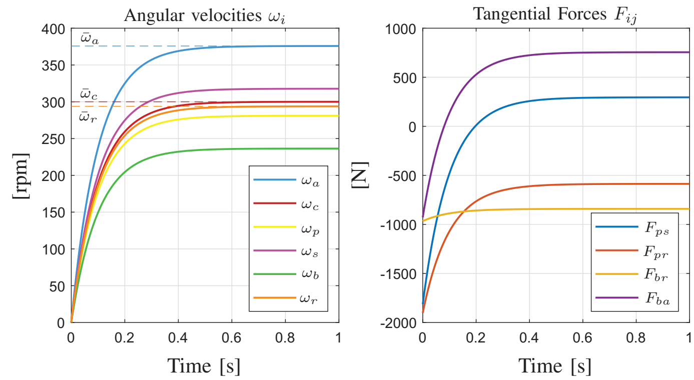

Fig. 8. Simulation of the Coupled epicyclic gear train: angular velocities ω_i (left subplot) and tangential forces F_{ij} (right subplot).

V. CONCLUSION

In this paper, the Power-Oriented Graphs modeling technique has been exploited as a tool for modeling epicyclic gear trains. Thanks to the proposed approach, a full dynamic model including the gears interaction and a reduced dynamic model could be obtained. When deriving the reduced model, the user can choose which angular velocities are going to compose the reduced state vector, and the time behavior of the tangential forces can still be obtained. The modeling and simulation of two epicyclic gear trains of interest in the automotive industry have been addressed, showing the effectiveness of the procedure. Finally, the design of a suitable control law allowing to achieve the desired velocity while minimizing the system dissipations has been presented.

REFERENCES

[1] J. Liu and H. Peng, "Modeling and control of a power-split hybrid vehicle", *IEEE Trans. Control Syst. Technol.*, vol. 16, no. 6, pp. 1242-1251, Nov. 2008.

[2] D. Tebaldi and R. Zanasi, "Modeling and control of a power-split hybrid propulsion system", *IECON*, Lisbon, Portugal, Oct. 14-17, 2019.

[3] J. M. Miller, "Hybrid electric vehicle propulsion system architectures of the e-CVT type", *IEEE Trans. Power Electron.*, vol. 21, no. 3, pp. 756-767, May 2006.

[4] H. Jingnan, W. Shaohong, M. Chao, "Nonlinear dynamic analysis of 2K-H planetary gear transmission system", *ICEMI*, Yangzhou, China, Oct. 2017.

[5] Q. Tao, J. Zhou, W. Sun, J. Kang, "Study on the Inherent Characteristics of Planetary Gear Transmissions", *ICAC*, Glasgow, UK, Sept. 2015.

[6] X. Zhang, H. Peng, J. Sun, S. Li, "Automated Modeling and Mode Screening for Exhaustive Search of Double-Planetary-Gear Power Split Hybrid Powertrains", ASME Dynamic Systems and Control Conference, San Antonio, Texas, Oct 22-24, 2014.

[7] H. L. Benford and M. B. Leising, "The level analogy: a new tool in transmission an alysis", *SAE Trans.*, vol. 90, no. 1, pp. 429-437, 1981.

[8] R. Zanasi, G. H. Geitner, A. Bouscayrol, and W. Lhomme,"Different energetic techniques for modelling traction drives", *ELECTRIMACS*, Québec, Canada, Jun. 8-11, 2008.

[9] R. Zanasi and D. Tebaldi, "Planetary gear modeling using the power-oriented graphs technique", *ECC*, Naples, Italy, Jun. 25-28, 2019.

[10] R. Zanasi, "The power-oriented graphs technique: system modeling and basic properties", *VPPC*, Lille, France, Sep. 1-3, 2010.